Alteration of Strain Distribution in Distal Tibia After Triple Arthrodesis: Experimental and Finite Element Investigations

Ahmad Chitsazan[a], Walter Herzog[b], Gholamreza Rouhi[a*], Mostafa Abbasi[c]

Running title: Biomechanical Considerations in Ankle Joint with Triple Arthrodesis

[a]*Faculty of Biomedical Engineering, Amirkabir University of Technology, 424 Hafez Ave., Tehran 1591634311, Iran*
[b]*Faculty of Kinesiology, Human Performance Lab, University of Calgary, Calgary, Alberta, T2N 1N4, Canada*
[c]*Department of Mechanical and Materials Engineering, University of Denver, 2390 S. York St. #200 Denver, CO 80210, USA*

Abstract

Arthrodesis, or fusion of subtalar joints (STJs), is a well-accepted and a routine treatment in the end stage of ankle injuries or disorder, such as arthritis or fractures. Arthrodesis can restore daily life function quickly at the expense of limiting joint motion. A triple arthrodesis (TA) consists of the surgical fusion of the talocalcaneal (TC), talonavicular (TN), and calcaneocuboid (CC) joints in the foot. This study aimed at investigating the effects of TA on strain distribution around tibia near the ankle joint. A finite element (FE) model, generated using computed tomography (CT) images of the human ankle, was then used to estimate stress distribution on the ankle joint surface. Axial load was applied to a human cadaveric ankle before and after TA, and load patterns were determined in various anatomical positions by measuring strain distribution around the tibia. Therefore, the effects of fusion were investigated by comparing strain distribution obtained from experiment and from FE model before and following to fusion. A good agreement between the experiment and FE, for the mean value of experimentally measured strains per the strains determined by FEM was observed (1.4±0.32 before TA, and 1.51±0.49 after TA). Moreover, a well-accepted point-by-point comparison between FE results and experimentally measured strains was observed with a good correlation coefficient (r=0.94). Results of this study showed that: (1) there was a significant difference in strain magnitude and strain distribution around the tibia before and after TA; (2) the strain and stress were more uniformly distributed after fusion; and (3) the peak strain and stress values were shifted to the lateral and anterolateral portion of the tibia after the fusion. Results of this investigation showed that STJs fusion reduces the average values of strains around the cortical bone through changing the pattern of load transmission at the ankle joint.

Keywords: Ankle joint, Subtalar joints (STJs) fusion, Strain gauge, Strain and stress distribution, Experimental investigation, Finite element analysis (FEA)

[*]Corresponding author, Faculty of Biomedical Engineering, Amirkabir University of Technology,424 Hafez Avenue, Tehran, Iran. Tel: +98 21 64 54 2380, Fax: +98 21 66 46 8186
E-mail address: grouhi@aut.ac.ir OR grouhi@uottawa.ca

1. Introduction

The human ankle is a complex joint with motion in a polyarticular compartment [1,2]. In some studies, it has been suggested that the articular surfaces are the preliminary anterior/posterior stabilizers and also constrain inversion/eversion and internal/external rotation of the ankle [2,3]. It is well accepted that the articular contact area depends on the stability of the joint [4]. Factors that alter the articular contact area, such as a malunion or changes in the foot alignment, are thought to cause variations in load transfer across the joint, thereby altering the stress distribution on the articular surfaces [3,5]. Osteoarthritis and intra-articular fractures are the most common disorders at the ankle. Kakkar and Siddique showed that post-traumatic arthritis is the most common form of arthritis in the ankle, and tends to occur frequently in young patients [6]. As an important result, Mononen et al. found that the rapid degeneration has a meaningful relationship with osteoarthritis, which occurred quickly after the initiation of osteoarthritis [7]. Ankle arthrodesis (AA) is the classical treatment for ankle arthritis and other ankle injuries or diseases. The goal of arthrodesis is to fuse the ankle bones into one unit with the aim to relieve the pain. However, arthrodesis reduces the amount of motion at the joint. In many studies which were done on ankle osteoarthritis (AO) and its surgical treatment, i.e., AA and total ankle replacement (TAR), long term success, as well as alterations on biomechanics of the foot joints and biomechanical factors retrieval were investigated [8,9]. Although both surgical treatments are widely used, the decision making about them is still a challenge, because of their pros and cons. Even though, the AA has been successfully experienced over a century, nevertheless it alters the biomechanics of foot joints and may lead to subsequent arthritis in ankle neighbouring joints [10]. On the other hand, TAR causes less alteration of foot and ankle's biomechanics, but involves surgical complexities and is less promising on long term results. An ideal prosthesis for TAR has not yet been determined [11,12], and their subjectivity and the diversity of results over studies questioned their validity and reliability [13-15]. The lack of long-term success has been associated with biomechanical factors, thus the ankle biomechanics should be carefully considered in the planning of TAR. Factors such as, the age of patients, and the presence of degenerative changes in other joints, such as the subtalar, mid-tarsal, knee, hip, and the contra-lateral ankle should be taken into account, when performing TAR [16].

TA was introduced in 1923 as a fusion of the TC, TN, and CC joints [17]. The goal of TA was to create a well-aligned, plantigrade, and stable foot that allows patients with paralytic or deforming conditions to function better. The most common indications for TA were to correct lower extremity deformities in children resulting from poliomyelitis, cerebral palsy, Charcot-Marie-Tooth disease, clubfoot, and tuberculosis. In adults, TA was used following trauma, or in patients with degenerative arthritis, posttraumatic arthritis, neuromuscular disease, and tendon dysfunction [18]. It was shown that eight years after ankle fusion, approximately 50% of the patients have clinically significant hind foot arthritis [19], and after an average of 22 years, virtually all patients develop hind foot arthritis [20].

The stress protection and stress shielding in the ankle, following internal and external fixation, has been measured indirectly using strain measurements on bones [21,22]. In order to measure joint contact pressures directly, scientists have used pressure-sensitive film, or pressure transducers mounted at, or below the joint surface [3, 23,24]. However, these experimental approaches have limitations because of the artefacts being introduced by the complex shape of the articular surfaces, the introduction of measurement devices into the joint space, limitations of spatial and

temporal resolution, and the removal and compromise of structural components of the joint [3,25-28]. Measurement of strain in bone may help increase our understanding of the load distribution in the target joint, and indirectly help understanding the stress distribution in neighbouring joints [22]. As arthrodesis is still the most common approach in the treatment of ankle fractures, determination of contact area, load transfer, and stress distribution as a function of bone alignment, and foot stability are required in helping our understanding of the pathogenesis of degenerative disorders [3,23].

The main and primary goal of this work was to investigate how the strain distribution in tibia changes after triple arthrodesis, and the secondary scope was to see how load transmission path after the fusion can affect the stress distribution at the articular surface of the ankle. A 3-dimensional finite element (3-D FE) model was used to simulate STJ fusions, along with six strain gauges mounted around the tibia adjacent to the joint. The FE results, with the scope of verifying the theoretical model, were then compared with experimental data collected by strain gauges. Finally, in order to compare the stress distribution between a normal joint and TA, the verified FE model was used to find the stress distribution at the ankle articular surface, for the neutral position of foot, both in normal and following TA.

2. Methods

In order to investigate the effects of the physiological loads carried out by the bones, it is necessary to measure the bone strain "in-vivo", or to simulate it by loading models "in-vitro". Assessment of strain is an easy method when the appropriate technique is used [21]. As bone surface strain is a strong indicator of the bone's response to mechanical loading [29], analysis of the strain patterns around the bone, along the long axis of the diaphysis of bone, can provide useful information about the load transferring path. Eccentricity in the load, caused by altering STJs configuration before and after fusion, by a custom-designed fixture for five different positions of the foot, i.e. neutral, inversion, eversion, plantar flexion, and dorsi flexion make changes in the load transferring path, and produce bending effects, which can be sensed by strain gauges mounted around tibia near the ankle joint. The strain during loading and unloading was measured using six strain gauges attached around tibia close to the tibiotalar joint [27-31]. A FE model, generated from CT images of the ankle was made and validated by comparing the experimental data collected by the strain gauges with the strains resulted from the FE model. The stress distribution on the ankle articular surfaces was then estimated using the validated FE model in both normal joint and following TA in neutral position of the foot.

2.1 In-vitro experiment

A foot from a 46-year-old male cadaver with a healthy ankle joint was used for the experiments. After thawing the specimen at room temperature, soft tissues were carefully removed by an orthopaedic surgeon, while the joint capsule, cartilage and ligaments were left intact. The tibia was prepared by carefully removing the periosteal layer in order to attach the strain gauges Fig. 1(a). Six sensors (3 axes TML, Tokyo Sokki Kenkyujo Co., Ltd. rosette strain gauge) were carefully attached to the sub-layer of the periosteum Fig. 1(b). Two strain gauges were mounted on the anterior, two on the posterior, one on the medial, and one on the lateral side of tibia Fig. 1 (c,d)[5]. The primary axis of all strain gauges was placed along the longitudinal axis of the tibia, and the position of the strain gauges was

carefully selected in order to obtain optimal results near the ankle joint. Since the fibula is not a significant load bearing bone [32], it was neglected in the experimental loading and in the computational model.

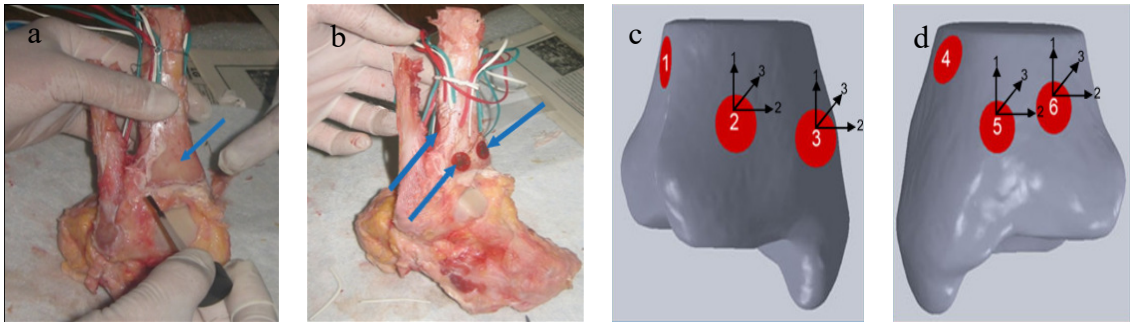

Fig. 1: a) Placement of the strain gauges on the tibia. Blue arrow shows the prepared area for mounting the sensors. b) Strain gauges were mounted on the anterior and lateral side of the tibia. c,d) Strain gauges arrangement at the distal end of the tibia. Sensors were attached near the joint surface on the tibial shaft near the ankle joint. c: lateral (1), anterolateral (2), and anteromedial (3); d: medial (4), posteromedial (5), and posterolateral (6) [5].

As shown schematically in Fig. 2 (left), the specimen was constrained at the proximal end of the tibia and load was applied from the bottom over a time period of about 40 seconds, from 0N to a maximum of 1000N, and then the load was gradually decreased to 0N in a custom- made fixture which was designed and fabricated in this study, in order to make the specimen stable without any motion during the tests. Utilizing this fixture, 30° plantar flexion, 20° dorsiflexion, and 15° inversion/eversion were attained in the foot, and the foot was accurately fixed on the top surface of the fixture through fastening some belts around the fixture. Strains were recorded by a TML, TDS 602 strain data logger throughout the loading and unloading periods [31].

Four orthopedic pins (Schanz screw) were inserted by an orthopedic surgeon for the fusion. Two pins were used for the fusion of talocalcaneal joint (TCJ), one for the calcaneocuboid joint (CCJ), and one for the talonavicular joint (TNJ) Fig. 2(right). Load was then applied to the fused ankle in the same manner as described above for the normal joint.

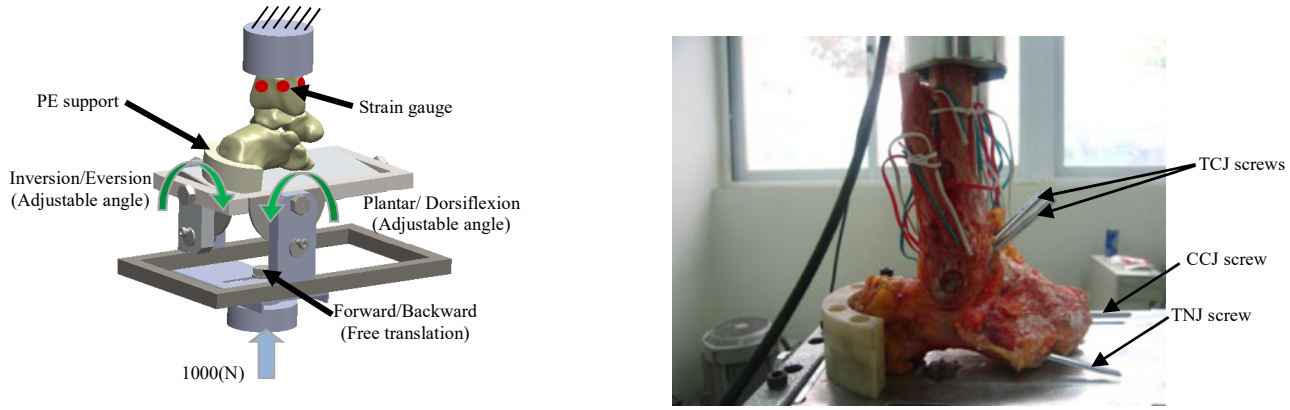

Fig. 2: Left: Experimental set up used in this investigation. The fixture was designed and manufactured in order to keep ankle fixed in various positions when loaded. **Right:** Total fusion of subtalar joints. TCJ was fused by two screws. TNJ and CCJ were fused each by one screw

2.2 Computational model

A 3D model of the foot and ankle was made using CT images. SIEMENS High Resolution multi-slice CT Scanner (SIEMENS^{TM}) was used to find out the CT scanning of a 46-year-old male, consisting a total number of 180 slices, pixel size of 0.354 mm, slice thickness of 0.6mm, current of 105 mA, voltage of 130 KV, and resolution of 512 x 512. Each bone was segmented in MIMICS software v.10.01 (The Materialise NV Inc. Belgium) and captured separately (tibia, talus, calcaneus, navicular, and cuboid) as a 3D shell. Then, CATIA (Dassault systems v.19) was used to remove uneven surfaces and to convert the bones into solid parts. In order to model articular cartilage, the smoothed surfaces of talus were extruded, normal to the surface, up to neighboring surface of tibia. In this case, a non-uniform thickness (between 0.65mm to 1.9mm) of articular cartilage was implemented that could be placed on the joint surface with a good fitness [33, 34]. FE modeling was performed using ANSYS (WORKBENCH V.13; ANSYS, PA, USA), and bones were imported into the Design Modeler module of ANSYS WORKBENCH as a deformable material [35]. All bones, except tibia, were assumed as linearly elastic and isotropic materials (Elastic modulus= 7300 MPa, and Poisson's ratio= 0.3) [36-42]. According to previous studies, load transmission at the distal tibia occurs mainly through the cortical rim [43] (Fig. 3), thus the tibia was modeled as a hollow shaft of cortical bone, which was segmented in CT images. The thickness of cortical bone, as expected, is not uniform and is position dependent (see Fig. 3) with orthotropic linear elastic material properties (Table 1) [42, 44]. The articular cartilage was modeled as a linear elastic and isotropic material (Elastic modulus= 12 MPa, Poisson's ratio= 0.42) [24, 45].

In order to model the normal ankle, the TCJs were given two degrees of freedom (DOF) in translation, and one DOF in rotation about the normal vector to the plane of the contact surface. The TNJ and CCJ were defined with three rotational DOF (Fig. 4). The TCJ was defined as a bonded contact with the contacting surfaces, which were assumed, affixed to each other. For modeling the fused ankle, all joints were modeled using bonded contacts.

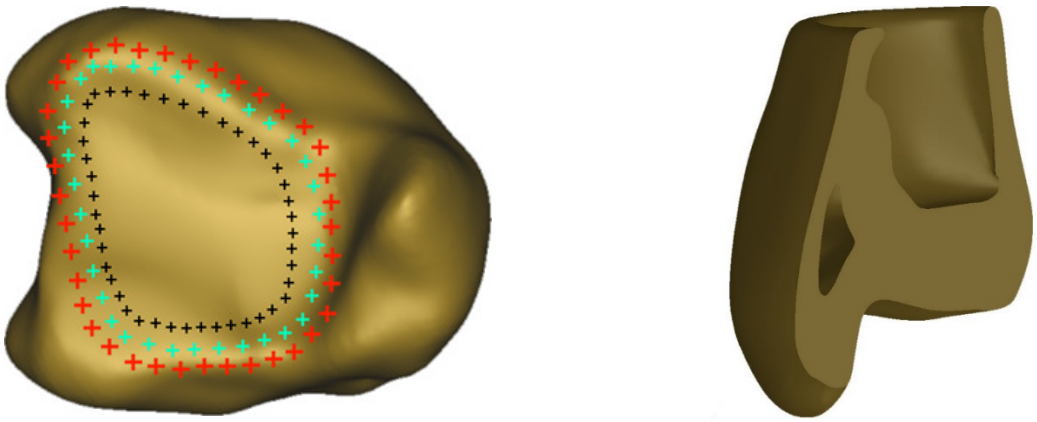

Fig. 3: Left: distal surface of the tibia. Load transmission at the distal tibia is thought to occur mainly through the cortical rim. The place of load exertion and the corresponding load intensity are indicated with the colored + signs. Red signs show a high magnitude of load transfer, green and black signs show medium and low magnitudes of load transfer, respectively [43]. Right: section view of the non-uniform thickness of cortical bone in distal tibia

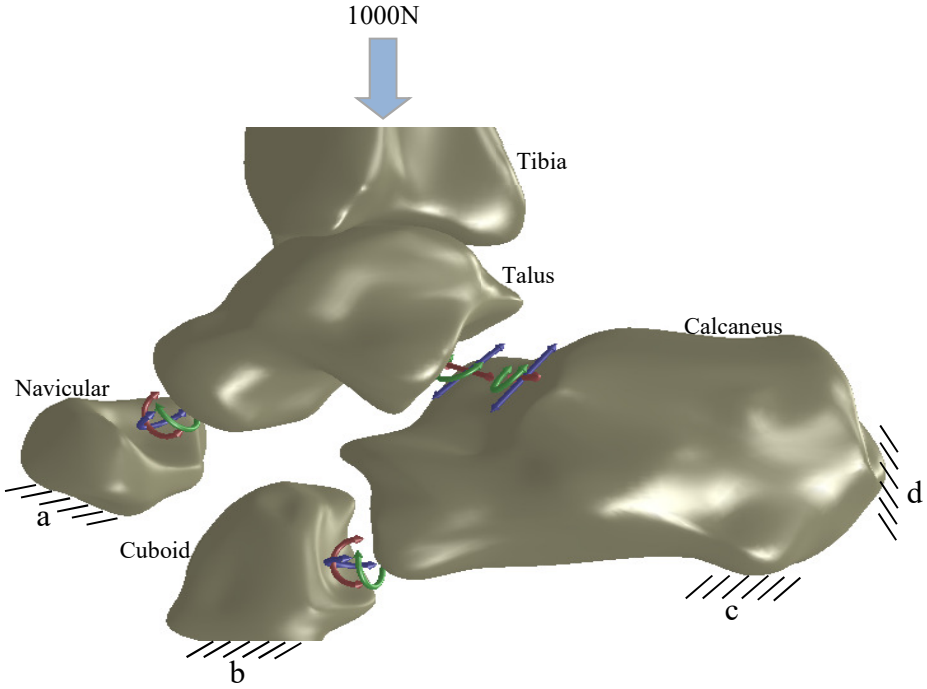

Fig. 4: Degrees of freedom considered for the normal subtalar joints. The talocalcaneal joint is considered as having two translational and one rotational DOF, while the talonavicular and the calcaneocuboid joints are defined with three rotational DOFs. Three fixed constraints, labeled as "a","b","c" considered on calcaneus, cuboid, and navicular, respectively. One non-frictional constraint in the place of "d" plays the role of PE support in the fixture (Fig. 2 (left))

Table 1: Mechanical properties of the human tibia. E_i and G_{ij} are in GPa, and orthotropic symmetry was assumed for the cortical bone [42]. E_3 is the modulus of elasticity in the tibia's longitudinal direction

Tissue type	**Material parameters**								
	E_1	E_2	E_3	G_{12}	G_{13}	G_{23}	ν_{12}	ν_{13}	ν_{23}
Tibia	6.91	8.51	18.4	2.41	3.56	4.91	0.49	0.12	0.14

3D SOLID187 element was used for meshing the bones (Fig. 5), and the mesh size varied between 1 and 3mm, depending on the bone curvature. TARGET170 and CONTACT174 elements were used for meshing the corresponding articular contact surfaces. Nonlinear spring elements (COMBIN39) were used for modeling the ankle ligaments. Ligaments were assumed to carry just tensile loading with a spring stiffness of 100 N/mm [46], and their spatial arrangements were in accordance with their anatomical locations (Fig. 5) [47]. For the sake of simplicity, muscles and tendons were neglected in our analyses, thus reaction forces are transferred via the joint surfaces exclusively [4,43].

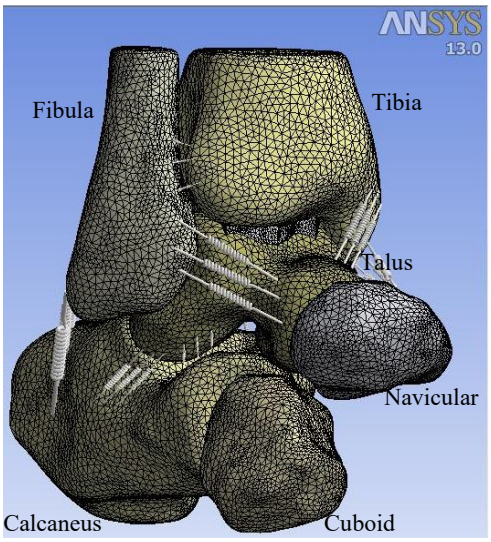

Fig. 5: Finite element model assembly. 3D SOLID187 elements in ANSYS were used for the bony mesh generation. Nonlinear spring elements, COMBIN39, were used for modeling the ligaments surrounding the joint. Fourteen ligaments (AT, PT, CF, PTF, ATF, ATC, ITC, PTT, TC, TN, ATT, MTC, PTC, DTN) were considered. Each ligament was modeled by three springs to avoid stress concentrations.

A mesh convergence study was performed to ensure that FE results are confident enough. Several simulations with different number of elements were performed and the minimum and maximum number of elements tested were 33935 and 556433, respectively, and an optimal number of elements for meshing was chosen to be 354649, for normal joint, and 320986, for Fused STJs, in this study. Load was applied, from the proximal end of tibia, and the foot was constrained at the bottom of the foot (Fig. 4). The rosette strain data (ε_1, ε_2, ε_3) were transferred to in-plane principal strains ($\varepsilon_{\text{Min.principal strain}}$, $\varepsilon_{\text{Max.principal strain}}$) by using Eqs. (1) and (2) [48]. von Mises strain was employed as the convergence criterion for the tibia. After calculating principal strains, von Mises strains, obtained by using Eq. (3), were determined, and were used to compare with the von Mises strains calculated in the FE model.

$$\boldsymbol{\varepsilon_{Max\ principal\ strain}} = \frac{1}{2}\left[\boldsymbol{\varepsilon_1 + \varepsilon_2 + \sqrt{2\{(\varepsilon_1 - \varepsilon_3)^2 + (\varepsilon_2 - \varepsilon_3)^2\}}}\right] \quad (1)$$

$$\boldsymbol{\varepsilon_{Min\ principal\ strain}} = \frac{1}{2}\left[\boldsymbol{\varepsilon_1 + \varepsilon_2 - \sqrt{2\{(\varepsilon_1 - \varepsilon_3)^2 + (\varepsilon_2 - \varepsilon_3)^2\}}}\right] \quad (2)$$

$$\boldsymbol{\varepsilon_{Von\ Mises}} = \sqrt{\left(\boldsymbol{\varepsilon_{Max\ principal\ strain}}\right)^2 + \left(\boldsymbol{\varepsilon_{Min\ principal\ strain}}\right)^2 - \boldsymbol{\varepsilon_{Max\ principal\ strain} * \varepsilon_{Min\ principal\ strain}}} \quad (3)$$

3 Results

Fig. 6(a)-(b) show the strains data collected by the lateral(a) and medial(b) strain gauges, i.e. strain gauges #1 and #4 in Fig. 1(c)-(d), for normal STJs and following TA conditions. As can be seen in Fig. 6(a)-(b), strain increased gradually to the peak value at the maximum load, and then returned steadily to the initial value upon unloading, which is in agreement with the strain analyses performed in prior studies [20,49].

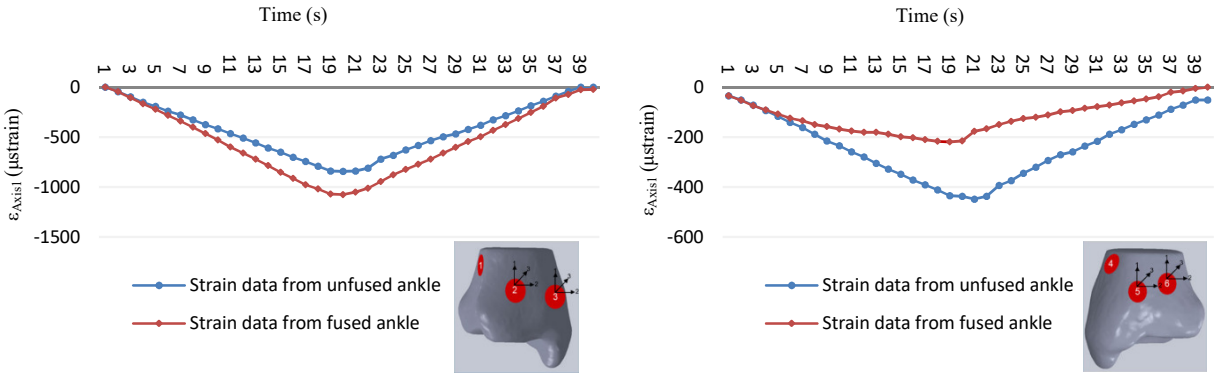

Fig. 6: Strains measured during the loading and unloading phases over a 40 second period. Loading went from 0N to 1000N, and unloading from 1000N to 0N. Results are shown for strain gauges from the lateral side of the tibia (strain gauge # 1) (left), and medial side of the tibia (strain gauge # 4) (right) for the normal and fused STJ conditions.

Tables 2 and 3 show strain gauges' data, minimum and maximum principal strains, and von Mises strains, for both normal and following TA, respectively, with the foot in a neutral position. The maximum and minimum values of von Mises strains after STJ fusion can be found at the lateral and posterolateral side of the tibia, respectively (lateral= 1322 με, posterolateral= 109 με). However, the maximum and minimum changes in von Mises strain following STJ fusion occurred at the posteromedial and posterolateral sides of the tibia, respectively. Posterolateral and posteromedial sides experienced strains of 8 με and 280.8 με, respectively.

Table 2: Maximum strain recorded by strain gauges for 1000N loading in the neutral foot position before TA. Minus signs indicate compressive strain

	ε_{Axis1} (μ strain)	ε_{Axis2} (μ strain)	ε_{Axis3} (μ strain)	$\varepsilon_{max.\ principal\ strain}$ (μ strain)	$\varepsilon_{min.\ principal\ strain}$ (μ strain)	$\varepsilon_{vonMises}$ (μ strain)

Medial	-414	208	-218	229	-435	584.2
Anteromedial	-528	324	-324	378	-582	837.6
Anterolateral	-334	381	178	413	-366	675.0
Lateral	-843	334	-143	344	-853	1067.4
Posterolateral	-52	82	13	82	-52	117.0
Posteromedial	-282	356	46	356	-282	553.8
Mean ± SD	408.8±242.1	280.8±104.2	74.6±170	300.3±112.9	428.3±248.6	639.1±290.6

Table 3: Maximum strains recorded by strain gauges for 1000N loading in neutral foot position after TA. Minus signs indicate compressive strain

	ε_{Axis1} (μstrain)	ε_{Axis2} (μstrain)	ε_{Axis3} (μstrain)	$\varepsilon_{max.\ principal\ strain}$ (μstrain)	$\varepsilon_{min.\ principal\ strain}$ (μstrain)	$\varepsilon_{vonMises}$ (μstrain)
Medial	-185	162	61	177	-200	326
Anteromedial	-484	290	-290	335	-529	755
Anterolateral	-504	495	61	499	-508	873
Lateral	-1070	383	-221	393	-1080	1322
Posterolateral	-46	61	40	70	-55	109
Posteromedial	-130	181	48	183	-132	273
Mean ± SD	403.1±344.2	262±145.3	50.1±146.7	276.1±145.9	-417.3±346.3	609.6±416.8

In table 4, von-Mises strains calculated using strain gauge data and equations 1 to 3, used for comparing with FE results in both normal STJs and following TA, can be found.

Table 4: von Mises strains (μstrain) determined using strain gauges vs. strains found by FE model for the normal and following TA

	von Mises strains (FEM)		von Mises strains (Experiment)	
	Normal STJs	TA	Normal STJs	TA
Medial	465	293	584.2	326
Anteromedial	578	560	837.6	755
Anterolateral	323	345	675.0	873
Lateral	841	894	1067.4	1322
Posterolateral	92	70	117.0	109
Posteromedial	503	261	553.8	273

Figure 7 shows von Mises strain under maximum loading measured and computed using FEM data for both normal joint and TA, and table 5 shows the strain ratio, as a comparative index for each strain gauge, using data

reported in this figure. The average and standard deviation (SD) for each set of data (normal and TA) can be found in table 5, which shows a good conformity of data for each position.

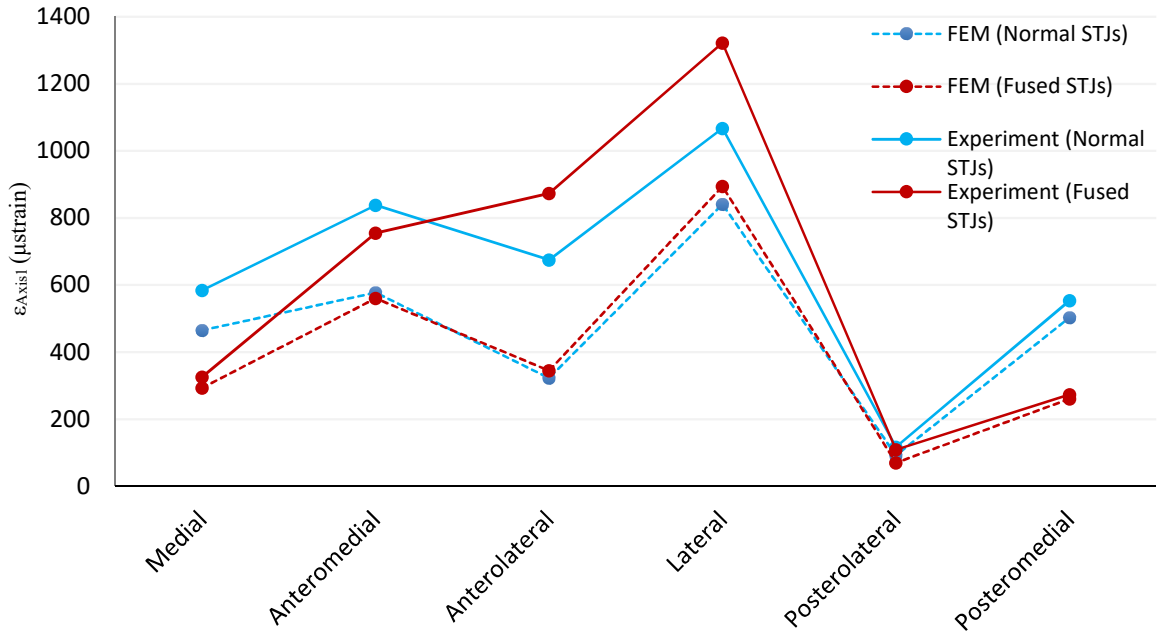

Fig. 7: The maximum strain measured by strain gauge and computed by FEM in both normal STJs and TA

Table 5: Strain ratio, i.e. experimentally measured strain per strain resulted from FEM, for each strain gauge using data shown in fig. 7

	Experimentally Measure Strain/ Strain resulted from FEM						**Average ± SD**
	Medial	Anteromedial	Anterolateral	Lateral	Posterolateral	Posteromedial	
Normal STJs	1.256	1.449	2.090	1.269	1.272	1.101	1.4±0.32
TA	1.113	1.348	2.530	1.479	1.557	1.046	1.51±0.49

Changes in strain ratio around the tibia, as a ratio of TA to normal STJs, both for the experimental data and FE results, can be seen in Fig. 8. As can be seen in this figure, following STJ fusion, the strains were transferred from the medial, anteromedial and posteromedial sides of the ankle to the lateral and anterolateral aspects of the ankle. Tables 6 and 7 show von Mises strains collected by the strain gauges for both normal STJs and following TA.

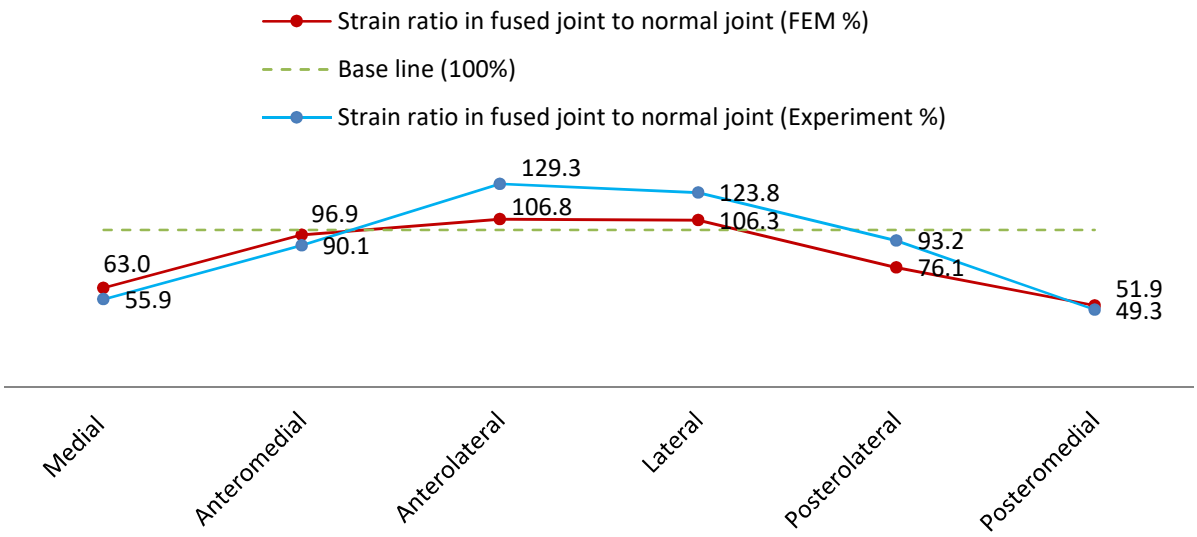

Fig. 8: Strain ratio, i.e., strain in the fused subtalar joint divided by the strain in the normal joint, obtained by strain gauges (blue) and FE model (red)

Table 6: von Mises strains for the normal joint in the different positions of the foot. Data were calculated using the raw data (similar to table 3) measured by the strain gauges mounted on the tibia

von Mises strain before TA (µstrain)						
	Level	Plantar flexion	Dorsi flexion	Inversion	Eversion	Average ±SD
Medial	584.2	537	445	557	183	461.24 ±146.7
Anteromedial	837.6	1123	931	1088	1130	1021.92±117
Anterolateral	675.0	689	742	767	1183	811.2±188.9
Lateral	1067.4	1048	1365	994	1614	1217.68±236.7
Posterolateral	117.0	1892	130	106	180	485±703.9
Posteromedial	553.8	902	3345	386	668	1170.96±1099.8
Average ±SD	639.1±290.7	1031.8±433.5	1159.6±1050	649.6±341.1	826.3±531.7	

Table 7: von Mises strain after TA in the different positions of the foot. Data were calculated using the raw data (similar to table 3) measured by the strain gauges mounted on the tibia

von Mises strain after TA (µstrain)						
	Level	Plantar flexion	Dorsi flexion	Inversion	Eversion	Average ±SD
Medial	326	409	426	831	222	442.8±207.1
Anteromedial	755	613	501	1552	812	846.6±369.1
Anterolateral	873	793	1034	793	1509	1000.4±269
Lateral	1322	1520	1489	596	2031	1391.6±463.1
Posterolateral	109	94	161	170	210	148.8±42.2
Posteromedial	273	425	345	270	452	353±75.2
Average ±SD	609.6±416.8	642.3±446.5	659.3±457.4	702±452.4	872.6±681.8	

Figure 9 shows the von Mises stress distribution on the tibiotalar joint before (left) and after TA (right) in neutral position of foot. As can be seen in this figure, the maximum stress before TA occurs on the medial side of the joint surface, and it is about 10MPa, while after the fusion, the maximum stress is shifted laterally (>11MPa) in anterolateral side of the surface. Moreover, before TA, stress is concentrated on the anteromedial and anterolateral sides of the surface, while after fusion, stress distributed along the anterior side of the joint, as well as the rest of the surface which is indicated in the stress contours with more uniformity after the fusion (Fig. 9). Even though the maximum stress in the fused situation is greater than that of unfused state, but, as can be seen in Fig. 9, a more uniform stress distribution can be seen after fusion.

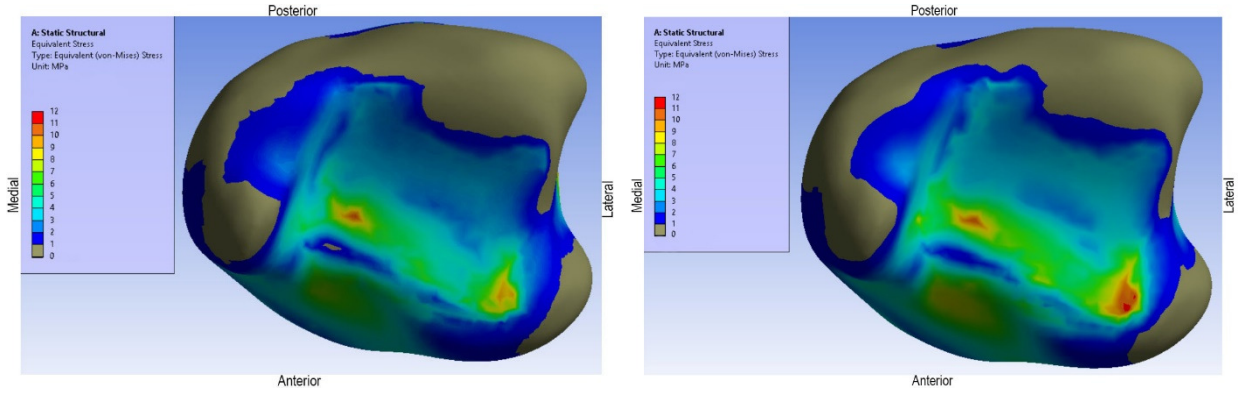

Fig. 9: Inferior view of the tibia, von Mises stress distribution on the tibiotalar joint. Left: before TA; Right: after TA

Figure 10 (left and right) show the von Mises strain under maximum loading for all positions acquired from the experiments, and for various posture of the ankle joint. Through comparing these two figures, one can be seen that an increase on lateral side of the joint, and a reduction on posterolateral and posteromedial after fusion.

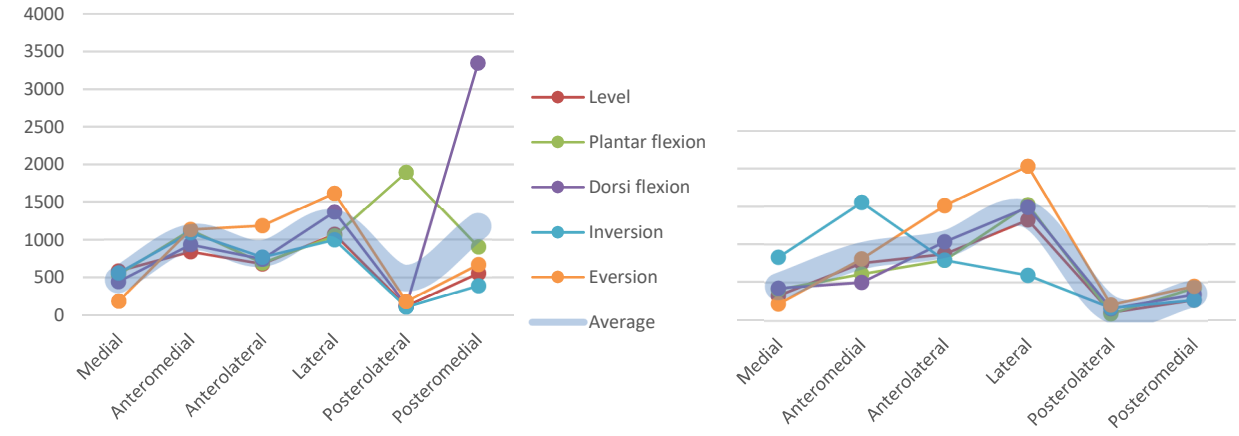

Fig. 10: von Mises strains under maximum loading collected by strain gauges versus different anatomical position, and for various posture of the ankle joint before (left) and following TA (right)

4 Discussion

Many studies have been performed investigating load transmission and contact pressure distribution in the ankle joint, and most of these studies used invasive approaches, particularly when they were focused on determining contact areas and stress distributions on the articular surfaces of the joint [50-52]. In this study, a new method was used to illustrate the effects of TA in the ankle utilizing experimental (using strain gauges), and computational (FEA) methods simultaneously to measure, and calculate strain distribution on the cortical shell of tibia, and to find stress distribution at the articular surfaces of the ankle prior to, and following TA.

In this study, it was found that for the neutral position of the foot, there were no significant differences in the average of strains between a normal STJs and following TA, whereas for the plantar and dorsi-flexed foot positions, the strains differed significantly (Tables 6, 7). Moreover, it was shown that following the fusion, the load transfer across the ankle was significantly changed (see tables 6 and 7). This change in the biomechanics of the ankle joint, associated with the fusion might be able to help explain the degenerative changes, post-operative pains, and arthritis in ankle following arthrodesis [18, 21, 49]. Comparing stress distribution before and following TA, it was found that, as shown in figure 9(left and right) and tables 6 and 7, the force transfer across the ankle is altered by the fusion. Also, it has been reported that ankle degeneration can be accelerated following TA [53,54], possibly due to transferring abnormal loads to the neighboring joints, and thus causing abnormal stress distribution at the neighboring joints' surfaces [53]. Following the fusion, the stress distribution was found to be more uniform, and was distributed over a greater area compared to that found for the normal joint condition (see Fig. 9). Post-operative tibial stress fracture after arthrodesis, which is known as a prevalent problem [52, 53], it can be likely caused by abnormal load transfer across the ankle components. Considering Fig. 10, which shows the von Mises strain under maximum loading for different positions on the joint, and for various postures, one can conclude that positioning the STJs components properly relative to the mechanical axis of the ankle, also with respect to each other during the surgery can be likely a crucial determinant in the fate of the ankle after surgery.

A point by point comparison between fused and normal joint in FEM and measured data (Fig. 8 and table 5) showed a good agreement between the experiment and FE simulation. Using Wilcoxon test [55, 56], differences were normally distributed with mean and standard deviations of 1.4±0.32 for the strain ratio (experiment/FEM strains) in normal STJs and 1.51±0.49 after the fusion.

Based on the normal distribution, experimental data and computational model results are highly correlated with $r=0.925$, $p=0.03$ for normal STJs, and $r=0.92$, $p=0.03$ for TA. Moreover, according to Fig. 8, the cumulative differences between experiment and computational model was $r=0.94$.

It is interesting to note that according von Mises strains (see tables 6 and 7), collected by strain gauges in different positions of the foot, there are no significant differences between normal STJs and TA, in three different positions, i.e. level (624.35 ±14.75), inversion (675.8±26.2), and eversion (849.45 ±23.15), whereas their components, i.e. strain corresponds to each position, are quite different in normal joint and after TA. Based on these results, it might be inferred that by making changes to STJs, just the pattern of the load transfers among different components of the joint would change, but the total amount of the strain will remain constant. On the other hand, the discrepancies in plantar flexion (837±194.75) and dorsi-flexion (909.4±250.15) can be due to the lack of enough number of strain

gauges mounted around tibia. In other words, if more strain gauges could be mounted around tibia to get more data, von Mises strains distribution could show a similar behavior in plantar and dorsi-flexion too.

There was no significant difference in the average of strains between normal STJs and following TA (tables 6, 7) in neutral, inversion and eversion positions of the foot. Whereas, for the plantar and dorsi-flexed foot positions, the average of the strains differed significantly between the normal and fused STJs conditions (tables 6, 7). As total amount of the external load was constant, it can be inferred that after the fusion, load transferring pattern was changed and distributed more uniformly so that was not logged in the place of the mounted strain gauge as well as before the fusion.

Results of this work are in agreement with the previous investigations such as: Tochigi and co-workers that suggested the articular surface restraints play a primary role in anterior/posterior, inversion/eversion, and internal/external rotation ankle stability [4]; or Kura and co-workers that showed the articular surface contact area depends on the position of the foot and the magnitude of the axial load [3]. Kura et al. found that for the neutral position of foot, anterior and anteromedial sides of the ankle transfer the main amount of the load, which is in agreement with our finding (Fig. 9).

One of the limitations of this study was the number of cadaver, i.e. 1, in the tests. It is clear by increasing the number of cadaver, one can make more solid conclusions based on the data collected in the in-vitro tests. Another limitation was to neglect the force transmission by the fibula. It is known that approximately 3.7% to 13.0% of the axial forces across the ankle is transferred via fibula [57], thus disregarding fibula, in this study, cannot cause considerable errors. Furthermore, ankle joint stress distributions were only calculated for the neutral position of foot, thus extrapolation of these results to other foot positions should be made with caution. Moreover, using bonded contacts for modeling fusion in ANSYS Workbench was based on the fact that after a couple of days of surgery, the fused joints will be transformed to a unified compartment [54]. In regard to the experiment, screws were assumed to act as the preliminarily fixators of the bones, which keep the bones connected to each other. Thus it was assumed that when static load is applied, different bones fused to each other by the screws, will have neither rotational, nor translational motion relative to each other It should be noted that in this work, the local effects of screw's insertion on the strain distribution within the bone was not taken into account. Finally, it should be noted that, in spite of the fact that in this study the FE model was made based on the geometry of a specimen different from the cadaver used in our experiments, a good agreement between the FEM and the experiment was found in the trend of strain distribution, adjacent to the ankle joint, around the tibia. This has encouraged us to draw the conclusion, in agreement with some previous studies [58, 59], that there might be a plausible similarity in human bone geometry from various individuals.

5 Conclusions

Results of this study indicate that load transferring pattern is highly sensitive to the anatomical position of the foot, and/or interventional operations, such as TA of the ankle joint. Moreover, it was shown that TA reduces the average values of strain on the cortical bone surface, through changing the pattern of load transmission. It was also shown that following TA, stress distribution is shifted from the medial side to the lateral side, with a more even distribution, compared to the normal STJs. In regard to the stress distribution, it was also found that after TA, the

maximum value of stress is greater than that of a normal joint, which can be deemed as a rough explanation for the post-operative disorders, in the ankle joint, after fusion, such as degenerative changes in the articular cartilage.

6 Acknowledgement

We acknowledge the support of the Iran National Science and Foundation (INSF) under grant No. 91004528, Iranian tissue bank center (ITB), and Amirkabir University of Technology. The authors also would like to acknowledge Dr. S. Pezeshki(orthopedic surgeon) for the arthrodesis surgery, and the help in medical imaging given by Mrs. S. Serajzadeh (technologist), of the department of imaging, Shafa Yahyaian Hospital, Iran University of Medical Sciences. Dr. Z. Ghayoumi's assistance on the statistical analyses is gratefully appreciated.

7 Conflict of interest

The authors have no conflict of interest to report.

8 References

1. Dettwylera, M., Stacoffa, A., Ine`s, A., Quervaina, K., Stu¨ssia, E. (2004). Modelling of the ankle joint complex. Reflections with regards to ankle prostheses. Journal of Foot and Ankle Surgery, 10, 109–19.
2. Ajai, S. (2011). A review of the STAR prosthetic system and the biomechanical considerations in total ankle replacements. Journal of Foot and Ankle Surgery, 17, 64–7.
3. Kura, H., Kitaoka, H. B., Luo, Z., An, K. (1998). Measurement of surface contact area of the ankle joint. Journal of Clinical Biomechanics, 13, 365-70.
4. Tochigi, Y., Rudert, M. J., Saltzman, C. L., Amendoula, A., Brown, T. D. (2006). Contribution of articular surface geometry to ankle stabilization. Journal of Bone & Joint Surgery, 88-A, 2704-13.
5. Chitsazan, A., Rouhi, G., Pezeshki, S., Abbasi, M., Tavakoli, A. H. (2015). Assessment of stress distribution in ankle joint: simultaneous application of experimental and finite element methods, Journal of International Experimental and Computational Biomechanics, 3(1),45-61.
6. Kakkar, R., Siddique, M. S. (2011). Stresses in the ankle joint and total ankle replacement design, Journal of Foot and Ankle Surgery, 17, 58-63.
7. Mononen, M. E., Tanska, P., Isaksson, H., Korhonen, R. K. (2016). A Novel method to simulate the progression of collagen degeneration of cartilage in the knee: data from the osteoarthritis initiative, Journal of Scintific Report. doi:10.1038/srep21415.
8. Campbell W. C., Crenshaw, A. H. (1987). Arthroplasty of ankle and knee. Campbell's operative orthopedics. St. Lois Mosby, 1145–50. ISBN: 0801610656 9780801610653.
9. Beyaert, C., Sirveaux, F., Paysant, J., Mole, D., Andre, J. M. (2004) The effect of tibio-talar arthrodesis on foot kinematics and ground reaction force progression during walking, Journal of Gait & Posture, 20, 84–91.
10. Thomas, R., Daniels, T. R., Parker, K. (2006). Gait analysis and functional outcomes following ankle arthrodesis for isolated ankle arthritis, American Journal of Bone and Joint Surgery, 88, 526–35.
11. Henne, T. D., Anderson, J.G. (2002). Total ankle arthroplasty: a historical perspective, Journal of Foot and Ankle Clinics, 7, 695–702.
12. Saltzman, C. L. (2000). Perspective on total ankle replacement, Journal of Foot and Ankle Clinics, 5, 761–75.
13. Button, G., Pinney, S. (2004). A meta-analysis of outcome rating scales in foot and ankle surgery: is there a valid, reliable, and responsive system?, Journal of Foot & Ankle International, 25, 521–25.
14. Herron, M. L. (2006). A review of outcome measures for the ankle and hindfoot, Journal of Foot and Ankle Surgery, 12, 161–7.
15. Naal, F. D., Impellizzeri, F. M., Rippstein, P. F. (2010). Which are the most frequently used outcome instruments in studies on total ankle arthroplasty?, Journal of Clinical Orthopaedics and Related Research, 468, 815–26.
16. Bonasia, D. E., Dettoni, F., Femino, J. E., Phisitkul, P., Germano, M., Amendola, A. (2010). Total ankle replacement: why, when and how?, Journal of Iowa Orthopeic, 30, 119–130.

17. Ryerson, E. W. (2008). Arthrodesing operations on the feet, Journal of Clinical Orthopaedics and Related Research, 466(1), 5-14.
18. Knupp, M., Stufkens, S. A., Hintermann, B. (2011). Triple arthrodesis, Journal of Foot Ankle Clinic, 16(1), 61-7.
19. Muir, D. C., Amendola, A., Saltzman, C. L. (2002). Long-term outcome of ankle arthrodesis, Journal of Foot and Ankle Clinics, 7(4), 703–8.
20. Coester, L. M., Saltzman, C. L., Leupold, J., Pontarelli, W. (2001). Long-term results following ankle arthrodesis for post-traumatic arthritis, Journal of Bone and Joint Surgery, 83, 219–228.
21. Cordey, J., Gautier, E. (1999). Strain gauges used in the mechanical testing of bones Part II: "In vitro" and "in vivo" technique, Journal of Injury, 30, SA14-20.
22. O'Doherty, D. M., Butler, S. P., Goodship, A.E. (1995). Stress protection due to external fixation system, Journal of Biomechanics, 28(5), 575-86.
23. Burke, N. G., Moran, C., Din, R., Walsh, J., Quinlan, W. R. (2010). An unusual cause of pain post ankle arthrodesis in patients with rheumatoid arthritis, Journal of The Foot, 20, 81–4.
24. Beaudoin, A. J., Fiore, S. M., Krause, W. R., Adelaar, R. S. (1991). Effect of isolated talocalcaneal fusion on contact in the ankle and talonavicular joints, Journal of Foot Ankle, 21(1), 19-25.
25. Anderson, D. D., Goldsworthy, J. K., Li, W., Rudert, M. J., Tochigi, Y., Brown, T. D. (2007). Physical validation of a patient-specific contact finite element model of the ankle, Journal of Biomechanics, 40, 1662-69.
26. Corazza, F., Stagni, R., Castelli, V. P., Leardini, A. (2005). Articular contact at the tibiotalar joint in passive flexion, Journal of Biomechanics, 38, 1205–12.
27. Chitsazan ,A., Rouhi, G., Pezeshki, S., Abbasi, M., Tavakoli, A. H. (2012). Strain distribution on tibia surface during gait cycle: experimental investigation, *Proc.CSB-SCB. Conf.*
28. Todd, O. M., Rudert, M. J., Koos, D. C., Pedersen, D. R., Baer, T.E., Tochigi, Y., Brown, T. D. (2006). Contact stress transients during functional loading of ankle step-off incongruities, Journal of Biomechanics, 39, 617–26.
29. Sugiyama, T., Meakin, L. B., Browne, W. J., Galea, G. L., Price, J. S., Lanyon, L. E. (2012). Bones' adaptive response to mechanical loading is essentially linear between the low strains associated with disuse and the high strains associated with the lamellar/woven bone transition, Journal of Bone Miner Research, 27(8),1784-93.
30. Perusek, P. G., Davis, L. B., Sferra, J. J., Courtney, C. A., D'Andrea, E. S. (2001). An extensometer for global measurement of bone strain suitable for use in vivo in humans, Journal of Biomechanics, 34, 385-91.
31. Gautier, E., Cordey, J. (1999). Strain gauges used in the mechanical testing of bones Part I: Theoretical and technical aspects, Journal of Injury, 30, SA7-13.
32. Levangie, P. K., Norkin, C. C. (2011). Joint structure and function: A comprehensive analysis. ISBN: 978-0-8036-2362-0, 440-78.
33. El-Khoury, G. Y., Alliman, K. J., Lundberg, H. J. (2004). Cartilage thickness in cadaveric ankles: measurement with double-contrast multi-detector row CT arthrography versus MR imaging, Journal of Radiology, 233, 768–73.
34. Li, W., Anderson, D. D., Goldsworthy, J. K., Marsh, J. L., Brown, T. D. (2008). Patient-specific finite element analysis of chronic contact stress exposure after intra-articular fracture of the tibial plafond, Journal of Orthopedic Research, 26, 1039-45.
35. Anderson, A. E., Ellis, B. J., Maas, S. A., Weiss, J. A. (2010). Effects of idealized joint geometry on finite element predictions of cartilage contact stresses in the hip, Journal of Biomechanics, 43(7), 1351-57.
36. Tao, K., Wang, D., Wang, C. h., Wang, X., Liu, A., Nester, Ch. J., Howard, D. (2009). An in vivo experimental validation of a computational model of human Foot, Journal of Bionic Engineering, 6, 387–97.
37. Chen, W. P., Tang, F. T., Ju, C. W. (2001). Stress distribution of the foot during mid-stance to push-off in barefoot gait: a 3-D finite element analysis, Journal of Clinical Biomechanics, 16(7), 614-20.
38. Gíslason, M. K., Stansfield, B., Nash, D. H. (2010). Finite element model creation and stability considerations of complex biological articulation: The human wrist joint, Journal of Medical Engineering and Physics, 32(5), 523-31.
39. Asgari, S. A., Hamouda, A. M. S., Mansor, J. B., Singh, H., Mahdi, E., Wirza, R., Prakash, B. (2004). Finite element modeling of a generic stemless hip implant design in comparison with conventional hip implants, Journal of Finite Element in Analysis and Design, 40, 2027-47.
40. Speirs, A. D., Heller, M. O., Duda, G. N., Taylor, W. R. (2007). Physiologically based boundary conditions in finite element modelling, Journal of Biomechanics, 40(10), 2318-23.
41. Taylor, W. R., Roland, E., Ploeg, H., Hertig, D., Klabunde, R., Warner, M. D., Hobatho, M. C., Rakotomanana, L., Clift, S. E. (2002). Determination of orthotropic bone elastic constants using FEA and modal analysis, Journal of Biomechanics, 35(6), 767-73.

42. Ionescu, I., Conway, T., Schonning, A., Almutairi, M., Nicholson, D. W. (2003). Solid modeling and static finite elemet analysis of the human tibia. *Conf. Bioengineering June 25-29 Florida.*
43. Hintermann, B. (2004). Total ankle arthroplasty: historical overview current concepts and future perspectives. ISBN: 978-3-211-27254-1, Wien, New York, Springer, 25-42.
44. Ragone, J. G. (2006). Finite element simulation of the MRTA test of a human tibia. Thesis for the degree of M.Sc in Biomedical Engineering and Sciences (BMES). Virginia polytechnic institute and state University. https://theses.lib.vt.edu/theses/available/etd-04202006-135139/unrestricted/Ragone_thesis_final.pdf
45. Anderson, D. D., Deshpande, B. R., Daniel, T. E., Baratz, M. E. (2005). A three-dimensional finite element model of the radiocarpal joint: distal radius fracture step-off and stress transfer, Journal of Iowa Orthopaedics, 25, 108–17.
46. Beumer, A., Hemert, W. L. W., Swierstra, B. A., Jasper, L. E., Belkoff, S. M. (2003). A biomechanical evaluation of the tibiofibular and tibiotalar ligaments of the ankle, Journal of foot & ankle international, 24(5), 426-29.
47. Anderson, A. E., Ellis, B. J., Maas, S. A., Peters, C. L., Weiss, J. A. (2008). Validation of finite element predictions of cartilage contact pressure in the human hip joint, Journal of Biomechanics 2008, 130(5), 1-25.
48. Young, W. C., Budynas, R. G. (2000). Roark's formulas for stress and strain. Seventh Edition. New York McGraw-Hill.
49. Cordey, J., Gautier, E. (1999). Strain gauges used in the mechanical testing of bones Part III Strain analysis, graphic determination of the neutral axis, Journal of Injury, 30, SA21-5.
50. Cristofolini, L., Conti, G., Juszczyk, M., Cremonini, S., VanSintJan, S., Viceconti, M. (2010). Structural behaviour and strain distribution of the long bones of the human lower limbs, Journal of Biomechanics, 40, 826–35.
51. Gíslason, M. K., Stansfield, B., Nash, D. H. (2010). Finite element model creation and stability considerations of complex biological articulation: The human wrist joint, Journal of Medical Engineering & Physics, 32, 523–31.
52. Easley, M. E., Vertullo, C. J., Urban, W. C., Nunley, J. A. (2002). Total ankle arthroplasty, Journal of American Academy of Orthopaedic Surgeons,10(3), 157-67.
53. Alvarez, R. (1996).Stress Fracture of the Tibia Following Extensive Hindfoot and Ankle Arthrodesis: A Report of Three Cases, Journal of Foot and Ankle International, 17(9), 583-584.
54. Groot, I. B., Reijman, M., Luning, H. A. F., Verhaar, J. A. N. (2008). Long-term results after a triple arthrodesis of the hindfoot: function and satisfaction in 36 patients, Journal of International Orthopaedics (SICOT), 32, 237–41.
55. Wilcoxon, F. (1945). Individual Comparisons by Ranking Methods. Biometrics Bulletin, 1(6): 80-3.
56. Hollander, M., Wolfe, D. A., Chicken, E. (1997). Nonparametric Statistical Methods. New York John Wiley & Sons 1997, 1st edition, 27-33 & 68-75.
57. Goh, J. C., Mech, A. M., Lee, E. H., Ang, E. J., Bayon, P., Pho, R. W. (1992). Biomechanical study on the load-bearing characteristics of the fibula and the effects of fibular resection, Journal of Clinical Orthopaedics Related Research, 279, 223-8.
58. Peacock, M., Buckwalter, K. A., Persohn, S., Hangartner, T. N., Econs, M. J., Hui, S. (2009). Race and Sex Differences in Bone Mineral Density and Geometry at the Femur, Journal of Bone, 45(2), 218–25.
59. Capozza, R. F., Feldman, S., Mortarino, P., Reina, P. S., Schiessl, H., Rittweger, J., Ferretti, J. L., Cointry, G. R., Structural analysis of the human tibia by tomographic (pQCT) serial scans, Journal of Anat, 216(4), 470–481.